CHAPTER 9 Aliasing instability

9.1 Aliasing error

Suppose that we have a wave given by the solid line in Fig. 9.1. The wave is plotted as

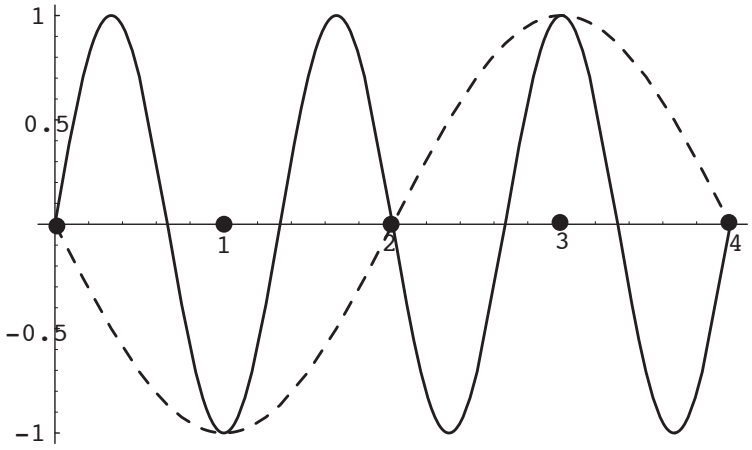

Figure 9.1: An example of aliasing error. Distance along the horizontal axis is measured in units of Δx. The wave given by the solid line has a wave length of $(4/3)\Delta x$. This is shorter than $2\Delta x$, and so the wave cannot be represented on the grid. Instead, the grid "sees" a wave of wavelength $4\Delta x$, as indicated by the dashed line. Note that the $4\Delta x$ -wave is "upside-down."

a continuous function of x, but at the same time we suppose that there are discrete, evenly spaced grid points along the x-axis, as shown by the black dots in the figure. The wave has been drawn with a wave length of $(4/3)\Delta x$. Because $(4/3)\Delta x < 2\Delta x$, the wave is too short to be represented on the grid. What the grid points "see" instead is not the wave represented by the solid line, but rather the wave of wavelength $4\Delta x$, as indicated by the dashed line (again drawn as a continuous function of x). At the grid points, the wave of length $4\Delta x$ takes exactly the values that the wave of $(4/3)\Delta x$ would take at those same grid points, if it could be represented on the grid at all. This misrepresentation of a wavelength too short to be represented on the grid is called "aliasing error." *Aliasing is a high wave number (or*

frequency) masquerading as a low wave number (or frequency). In the example of Fig. 9.1, aliasing occurs because the grid is too coarse to resolve the wave of length $(4/3)\Delta x$. Another way of saying this is that the wave is not adequately "sampled" by the grid. *Aliasing error is always due to inadequate sampling*.

Aliasing error can be important in observational studies, because observations taken "too far apart" in space (or time) can make a short wave (or high frequency) appear to be a longer wave (or lower frequency). Fig. 9.2 is an example, from real life. The blue curve in the

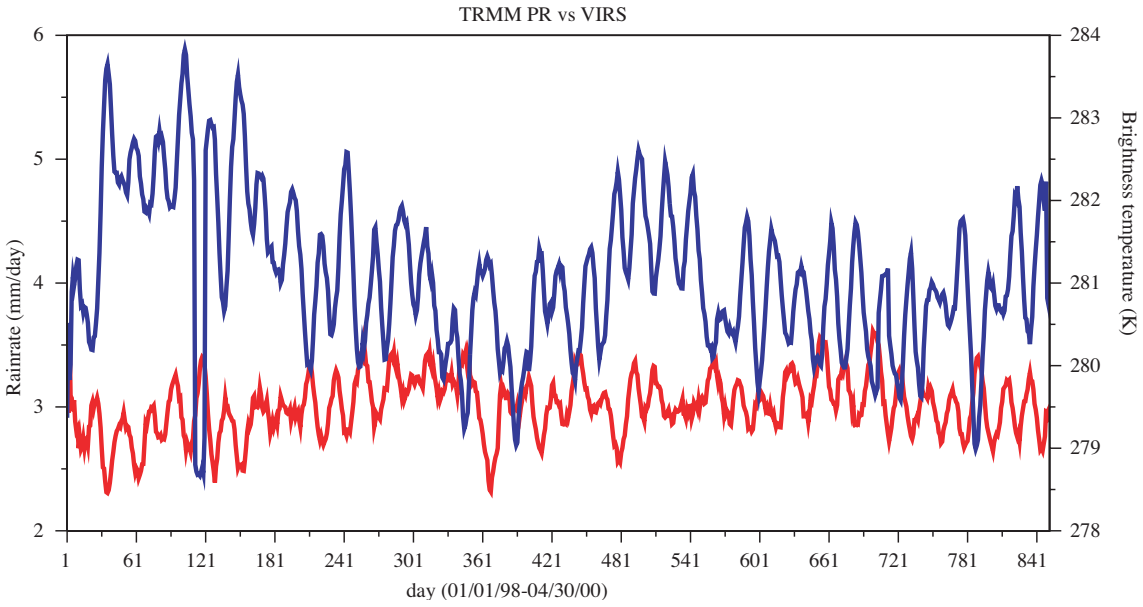

Figure 9.2: An example of aliasing in the analysis of observations. The blue curve shows the precipitation rate, averaged over the global tropics (20 S to 20 N), and the red curve shows a the thermal radiation in the 10.8 μm band, averaged over the same region. The horizontal axis is time, and the period covered is slightly more than two years. The data were obtained from the TRMM (Tropical Rain Mapping Mission) satellite. The obvious oscillation in both curves, with a period close to 23 days, is an artifact due to aliasing. See text for further explanation.

figure makes it appear that the precipitation rate averaged over the global tropics fluctuates with a period of 23 days and an amplitude approaching 1 mm day^{-1}. If this tropical precipitation oscillation (TPO) were real it would be one of the most amazing phenomena in atmospheric science, and its discoverer would be on the cover of *Rolling Stone*. But alas, the TPO is bogus, even though you can see it with your own eyes in Fig. 9.2, and even though the figure is based on real data, for goodness sake. The satellite from which the data was collected has an orbit that takes it over the same point on Earth *at the same time of day* once every 23 days. Large regions of the global tropics have a strong diurnal (i.e., day-night) oscillation of the precipitation rate. This high-frequency diurnal signal is aliased onto a much lower frequency, i.e., 23 days, because *the sampling by the satellite is inadequate* to resolve the diurnal cycle.

Aliasing error is also important in modeling, when we try to solve either non-linear equations or linear equations with variable coefficients. The reason is that the product terms (or other nonlinear terms) in such equations can produce, or try to produce, waves shorter

than the grid can represent. For example, suppose that we have two modes on a one-dimensional grid, given by

$$A(x_j) = \hat{A}e^{ikj\Delta x} \text{ and } B(x_j) = \hat{B}e^{ilj\Delta x}, \tag{9.1}$$

respectively. Here the wave numbers of A and B are denoted by k and l, respectively. We assume that k and l both "fit" on the grid in question. If we combine A and B linearly, e.g. form

$$\alpha A + \beta B, \tag{9.2}$$

where α and β are spatially constant coefficients, then no "new" waves are generated; k and l continue to be the only wave numbers present. In contrast, if we multiply A and B together, then we generate the new wave number, $k + l$:

$$AB = \hat{A}\hat{B}e^{i(k+l)j\Delta x}. \tag{9.3}$$

Other nonlinear operations such as division, exponentiation, etc., will also generate new wave numbers. It can easily happen that $(k + l)\Delta x > \pi$, in which case the new mode created by multiplying *A* and *B* together does not fit on the grid. *What actually happens in such a case is that the new mode is aliased onto a mode that* ***does*** *fit on the grid*.

Because the shortest wavelength that the grid can represent is $L = 2\Delta x$, the maximum representable wave number is $k_{max} \equiv \frac{\pi}{\Delta x}$. What happens when a wave with $k > k_{max}$ is produced, e.g. through nonlinear interactions? Since $2k_{max}\Delta x = 2\pi$, we can assume that $2k_{max} > k > k_{max}$. (A wave with $k > 2k_{max}$ "folds back.") We can write the expression $\sin(kj\Delta x)$ as

$$\begin{aligned} \sin(kj\Delta x) &= \sin[(2k_{max} - 2k_{max} + k)j\Delta x] \\ &= \sin[2\pi j - (2k_{max} - k)j\Delta x] \\ &= \sin[-(2k_{max} - k)j\Delta x] \\ &= \sin(k^* j\Delta x). \end{aligned} \tag{9.4}$$

where $k^* \equiv -(2k_{max} - k)$. (Question: What happens if $k < k_{max}$?) Similarly,

$$\cos[k(j\Delta x)] = \cos[k^*(j\Delta x)]. \tag{9.5}$$

This shows that the wave of wave number $k > k_{max}$ is interpreted (or misinterpreted) by the

grid as a wave of wave number $k^* \equiv -(2k_{max} - k)$. The minus sign means that the phase change per Δx is reversed, or "backwards". For $k > k_{max}$ we get $k^* < k_{max}$. For $k = k_{max}$, we get $k^* = k$.

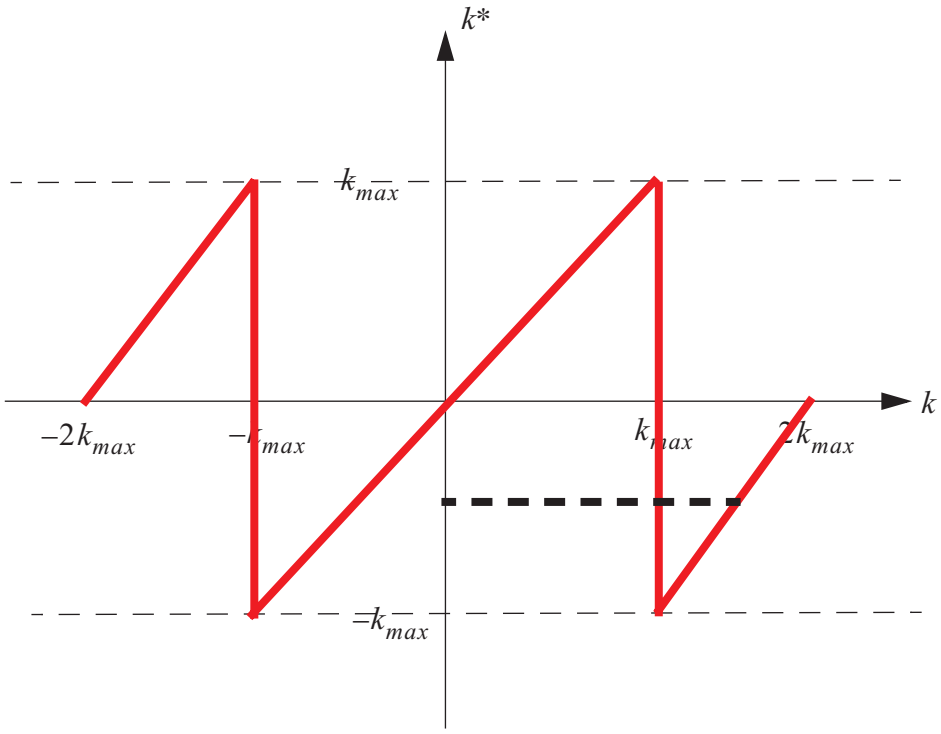

Figure 9.3: The red line is a plot of k^* versus k. The dashed black line connects $k = \frac{3}{2}\frac{\pi}{\Delta x}$ with $k^* = \frac{\pi}{2\Delta x}$, corresponding to the example of Fig. 9.1.

In the example of Fig. 9.1, $L = \frac{4}{3}\Delta x$ so $k = \frac{2\pi}{L} = \frac{2\pi\,3}{4\Delta x} = \frac{3}{2}\frac{\pi}{\Delta x}$. Therefore $k^* \equiv 2k_{max} - k = \frac{2\pi}{\Delta x} - \frac{3\pi}{2\Delta x} = \frac{\pi}{2\Delta x}$, which means that $L^* = 4\Delta x$, as we have already surmised by inspection of Fig. 9.1.

For $k < k_{max}$, the phase change, as j increases by one, is less than π. This is shown in Fig. 9.4 a. For $k > k_{max}$, the phase change as j increases by one is greater than π. This is shown in Fig. 9.4 b. The dot in the figure appears to move clockwise., i.e. "backwards." This is a manifestation of aliasing that is familiar from the movies. It also explains why the minus sign appears in Eq. (9.4).

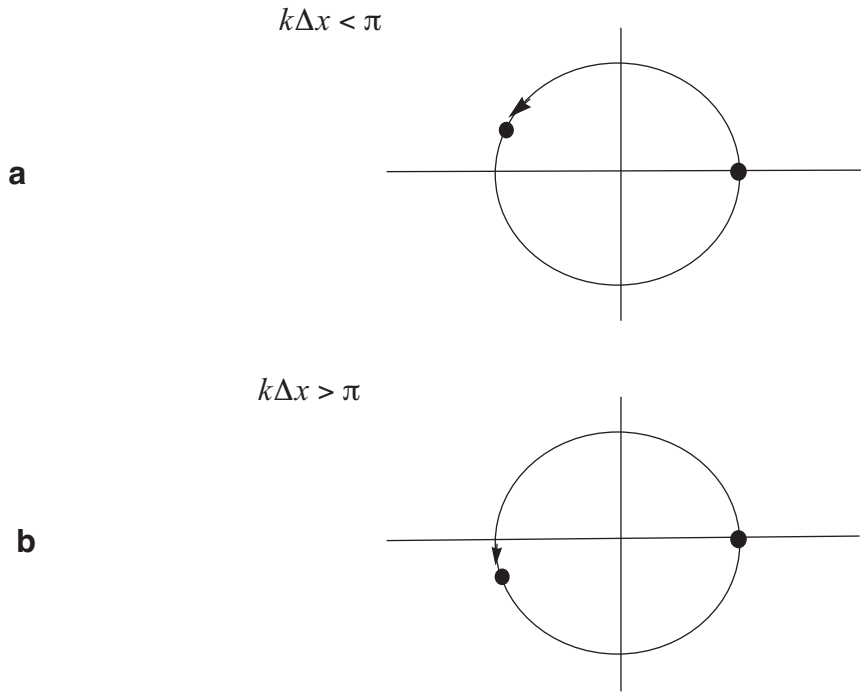

Figure 9.4: The phase change per grid point for: a) $k\Delta x < \pi$ **, and b)** $k\Delta x > \pi$ **.**

Aliasing error is important in part because it is the root cause of what is often called "nonlinear computational instability." This instability occurs with nonlinear equations, but as explained below it can also occur with linear equations that have spatially variable coefficients. A better name for the instability would be "aliasing instability." An example is presented in the next section.

9.2 Advection by a variable, non-divergent current

Suppose that an arbitrary variable q is advected in two dimensions on a plane, so that

$$\frac{\partial q}{\partial t} + \mathbf{v} \bullet \nabla q = 0 , \tag{9.6}$$

where the flow is assumed to be non-divergent, i.e.

$$\nabla \bullet \mathbf{v} = 0 . \tag{9.7}$$

Two-dimensional non-divergent flow is a not-too-drastic idealization of the large-scale circulation of the atmosphere. In view of (9.7), we can describe $\mathbf{v}$ in terms of a stream function ψ, such that

$$\mathbf{v} = \mathbf{k} \times \nabla\psi \,. \tag{9.8}$$

Substituting (9.6) into (9.6), we get

$$\frac{\partial q}{\partial t} + (\mathbf{k} \times \nabla\psi) \bullet \nabla q = 0 \,. \tag{9.9}$$

Using the vector identity

$$(\mathbf{V}_1 \times \mathbf{V}_2) \bullet \mathbf{V}_3 = \mathbf{V}_2 \bullet (\mathbf{V}_3 \times \mathbf{V}_1) \,, \tag{9.10}$$

which holds for any three vectors $\mathbf{V}_1, \mathbf{V}_2, \mathbf{V}_3$, we set $\mathbf{V}_2 \equiv \mathbf{k}$, $\mathbf{V}_1 \equiv \nabla\psi$, and $\mathbf{V}_3 \equiv \nabla q$, to obtain

$$(\nabla\psi \times \mathbf{k}) \bullet \nabla q = \mathbf{k} \bullet (\nabla q \times \nabla\psi) \,. \tag{9.11}$$

With the use of (9.11), we can re-write (9.6) as

$$\frac{\partial q}{\partial t} + J(\psi, q) = 0 \,, \tag{9.12}$$

or alternatively as

$$\frac{\partial q}{\partial t} = J(q, \psi) \,. \tag{9.13}$$

Here J is the Jacobian operator, which is defined by

$$\begin{aligned} J(p, q) &\equiv \mathbf{k} \bullet (\nabla p \times \nabla q) \\ &= -\mathbf{k} \bullet \nabla \times (q \nabla p) \quad , \\ &= \mathbf{k} \bullet \nabla \times (p e \nabla q) \quad , \end{aligned} \tag{9.14}$$

for arbitrary p and q. Note that

$$J(p, q) = -J(q, p) \quad , \tag{9.15}$$

which can be deduced from (9.14), and this has been used to pass from (9.12) to (9.13).

In Cartesian coordinates, we can write $J(q, \psi)$ in the following three alternative forms:

$$J(p, \psi) = \frac{\partial p}{\partial x}\frac{\partial q}{\partial y} - \frac{\partial p}{\partial y}\frac{\partial q}{\partial x} \tag{9.16}$$

$$= \frac{\partial}{\partial y}\left(q\frac{\partial p}{\partial x}\right) - \frac{\partial}{\partial x}\left(q\frac{\partial p}{\partial y}\right) \tag{9.17}$$

$$= \frac{\partial}{\partial x}\left(p\frac{\partial q}{\partial y}\right) - \frac{\partial}{\partial y}\left(p\frac{\partial q}{\partial x}\right) . \tag{9.18}$$

These will be used later.

Let an overbar denote an average over a two-dimensional domain which has no boundaries (e.g. a sphere or a torus), or on the boundary of which either p or q is constant. You should be able to prove the following:

$$\overline{J(p, q)} = 0 , \tag{9.19}$$

$$\overline{pJ(p, q)} = 0 , \tag{9.20}$$

$$\overline{qJ(p, q)} = 0 . \tag{9.21}$$

Multiplying both sides of (9.13) by q, we obtain

$$\frac{1}{2}\frac{\partial}{\partial t}q^2 = qJ(q, \psi) = J\left(\frac{1}{2}q^2, \psi\right) . \tag{9.22}$$

Integrating over the entire area, we see that

$$\int J\left(\frac{1}{2}q^2, \psi\right) ds = -\int \mathbf{v} \cdot \nabla \frac{1}{2}q^2 ds = -\int \nabla \cdot \left(\mathbf{v}\frac{1}{2}q^2\right) ds = 0 , \tag{9.23}$$

if the domain is surrounded by a rigid boundary where the normal component of **v** is zero, or if the domain is periodic.

When the stream function ψ is a prescribed function of the spatial coordinates, (9.13) is linear, although it has variable coefficients. As already mentioned, what is often called "non-linear" instability is actually a type of instability which can occur in the numerical integration of a linear equation with variable coefficients, as well as in the numerical integration of nonlinear equations. What this instability really amounts to is a spurious growth of waves due in part to the aliasing error arising from the multiplication of the finite difference analogs of *any* two spatially varying quantities.

To illustrate the problem, we begin by writing down a differential-difference version of (9.13), on a plane, using a simple finite-difference approximation for the Jacobian. For simplicity, we take $\Delta x = \Delta y = d$. We investigate the particular choice

$$\frac{dq_{i,j}}{dt} = [J_1(q,\psi)]_{i,j} \tag{9.24}$$

where

$$[J_1(q,\psi)]_{i,j} \equiv \frac{1}{4d^2}[(q_{i+1,j}-q_{i-1,j})(\psi_{i,j+1}-\psi_{i,j-1})-(q_{i,j+1}-q_{i,j-1})(\psi_{i+1,j}-\psi_{i-1,j})]\,. \tag{9.25}$$

You should confirm for yourself that (9.25) really is a finite-difference approximation to (9.13). In fact, it is modeled after (9.16). Later we are going to discuss several other finite-difference approximations for the Jacobian. The particular approximation given in (9.25) is called J_1. It will come up again in the later discussion.

Now we work through a simple example of aliasing instability, which was invented by Phillips (1959; also see Lilly, 1965). We combine (9.25) and (9.25) to obtain

$$\frac{dq_{i,j}}{dt} \equiv \frac{1}{4d^2}[(q_{i+1,j}-q_{i-1,j})(\psi_{i,j+1}-\psi_{i,j-1})-(q_{i,j+1}-q_{i,j-1})(\psi_{i+1,j}-\psi_{i-1,j})]\,. \tag{9.26}$$

Assume that the solution $q_{i,j}(t)$ is of the form

$$q_{i,j}(t) = \left[C(t)\cos\frac{\pi i}{2} + S(t)\sin\frac{\pi i}{2}\right]\sin\frac{2\pi j}{3}\,. \tag{9.27}$$

The use of such assumption may appear strange; it will be justified later. For all t, let $\psi_{i,j}$ be *prescribed* as

$$\psi_{i,j} = U\cos(\pi i)\sin\left(\frac{2\pi j}{3}\right)\,. \tag{9.28}$$

In (9.28), we are prescribing a time-independent but *spatially variable* advecting current. Earlier in the course we often prescribed the advecting current, but it was always spatially uniform. Because $\psi_{i,j}$ is prescribed, the model that we are considering here is linear. The forms of $q_{i,j}$ and $\psi_{i,j}$ given by (9.27) and (9.28) are plotted in Fig. 9.5.

Because (9.28) specifies $\psi_{i,j}$ to have a wavelength of $2d$ in the x-direction, we can simplify (9.25) to

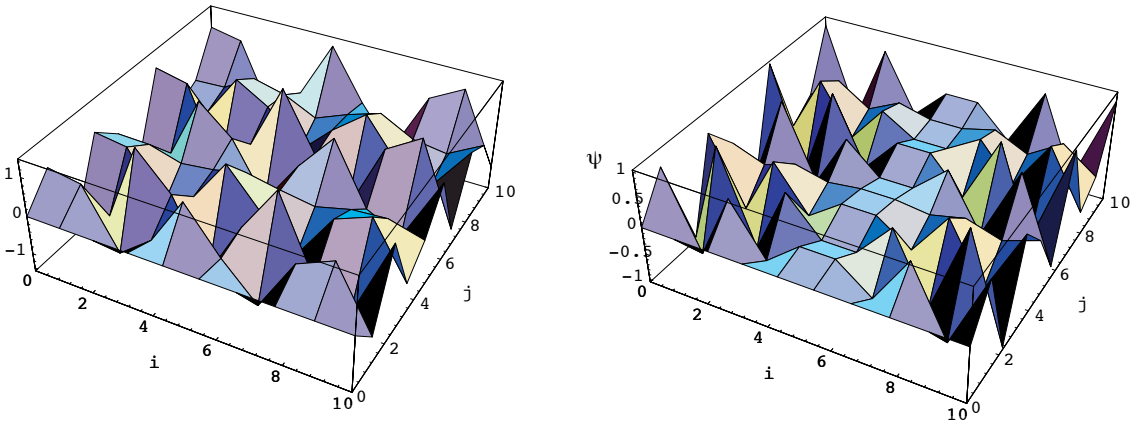

Figure 9.5: Plots of the functions q and ψ given by (9.27) and (9.28), respectively. For plotting purposes, we have used $C = S = U = 1$. The functions have been evaluated only for integer values of i and j, which gives them a jagged appearance. Nevertheless it is fair to say that they are rather ugly. This is the sort of thing that can appear in your simulations as a result of aliasing instability.

$$\frac{\partial q_{i,j}}{\partial t} = \frac{1}{4d^2}(q_{i+1,j} - q_{i-1,j})(\psi_{i,j+1} - \psi_{i,j-1}) \,. \tag{9.29}$$

From (9.27), we see that

$$\begin{aligned} & q_{i+1,j} - q_{i-1,j} \\ &= \left\{ C\left[\cos\frac{\pi(i+1)}{2} - \cos\frac{\pi(i-1)}{2} \right] + S\left[\sin\frac{\pi(i+1)}{2} - \sin\frac{\pi(i-1)}{2} \right] \right\} \sin\frac{2\pi j}{3} \\ &= 2\left(-C\sin\frac{\pi i}{2} + S\cos\frac{\pi i}{2} \right) \sin\frac{2\pi j}{3} \,. \end{aligned} \tag{9.30}$$

Here we have used some trigonometric identities. Similarly, we can show that

$$\psi_{i,j+1} - \psi_{i,j-1} = U\cos\pi i\left(2\cos\frac{2\pi j}{3}\sin\frac{2\pi}{3} \right) = \sqrt{3}\,U\cos\pi i\left(\cos\frac{2\pi j}{3} \right) \,. \tag{9.31}$$

As already mentioned, (9.31) holds for all t.

The product of (9.30) and (9.31) gives the right-hand side of (9.29), which can be written (again with the use of trigonometric identities) as

$$\frac{dq_{i,j}}{dt} = \frac{\sqrt{3}}{4d^2 2} U\left[-C\left(\sin\frac{3\pi i}{2} - \sin\frac{\pi i}{2}\right) + S\left(\cos\frac{3\pi i}{2} + \cos\frac{\pi i}{2}\right)\right]\sin\frac{4\pi i}{3}$$
$$= \frac{\sqrt{3}}{4d^2}\left(C\sin\frac{\pi i}{2} + S\cos\frac{\pi i}{2}\right)\sin\frac{4\pi j}{3}\,. \tag{9.32}$$

Note that

$$\frac{4\pi j}{3} = ly = l(jd)\,. \tag{9.33}$$

Therefore,

$$l = \frac{4\pi}{3d}\,. \tag{9.34}$$

This shows that the product on the right-hand side of (9.29) has produced a wave number in the y-direction of $l = \frac{4\pi}{3d} > l_{max} = \frac{\pi}{d}$, i.e., a wave too short to be represented on the grid. This wave will, according to our previous results, be interpreted by the grid as having wave number $-(2l_{max} - l) = -\left(\frac{2\pi}{3d}\right)$. Therefore (9.32) can be re-written as

$$\frac{dq_{i,j}}{dt} = -\left(\frac{\sqrt{3}U}{4d^2}\right)\left(C\sin\frac{\pi i}{2} + S\cos\frac{\pi i}{2}\right)\sin\frac{2\pi j}{3}\,. \tag{9.35}$$

Rewriting (9.32) as (9.35) is obviously a key step in this discussion, because it is where aliasing enters. In doing the problem algebraically, we have to put in the aliasing "by hand."

According to (9.35) the spatial form of $\frac{dq_{i,j}}{dt}$ agrees with the assumed form of $q_{i,j}$, given by (9.27). In other words, the spatial shape of $q_{i,j}$ does not change with time. *This justifies our assumption (9.27)*. In order to recognize that the spatial shape of $q_{i,j}$ does not change with time, we had to take into account that there will be aliasing.

If we now simply differentiate (9.27) with respect to time, and substitute the result into the left-hand side of (9.35), we get

$$\frac{dC}{dt}\cos\frac{\pi i}{2}\sin\frac{2\pi j}{3} + \frac{dS}{dt}\sin\frac{\pi i}{2}\sin\frac{2\pi j}{3} = -\frac{\sqrt{3}}{4d^2}U\left(C\sin\frac{\pi i}{2} + S\cos\pi\frac{i}{2}\right)\sin\frac{2\pi j}{3}\,. \tag{9.36}$$

Note that time derivatives of C and S appear on the left-hand side of (9.36). Using the linear

independence of the sine and cosine functions, we see from (9.36) that

$$\frac{dC}{dt} = -\frac{\sqrt{3}}{4d^2}US\,,\ \frac{dS}{dt} = -\frac{\sqrt{3}}{4d^2}UC\,. \tag{9.37}$$

From (9.37), it follows that

$$\frac{d^2C}{dt^2} = \sigma^2 C\,,\ \text{and}\ \frac{d^2S}{dt^2} = \sigma^2 S\,, \tag{9.38}$$

where $\sigma \equiv \frac{\sqrt{3}U}{4d^2}$. According to (9.38), C and S will grow exponentially. This demonstrates that the finite-difference scheme is unstable. The unstable modes will have the form given by (9.27).

Fig. 9.6 summarizes the mechanism of this aliasing instability. Nonlinear interactions feed energy into waves that cannot be represented on the grid. Aliasing causes this energy to "fold back" onto scales that do fit on the grid, but typically these are rather small scales that are not well resolved and suffer from large truncation errors. In the example given, the truncation errros lead to further production of energy on scales too small to be represented, etc. Note, however, that *if the numerical scheme conserved energy, the total amount of energy*

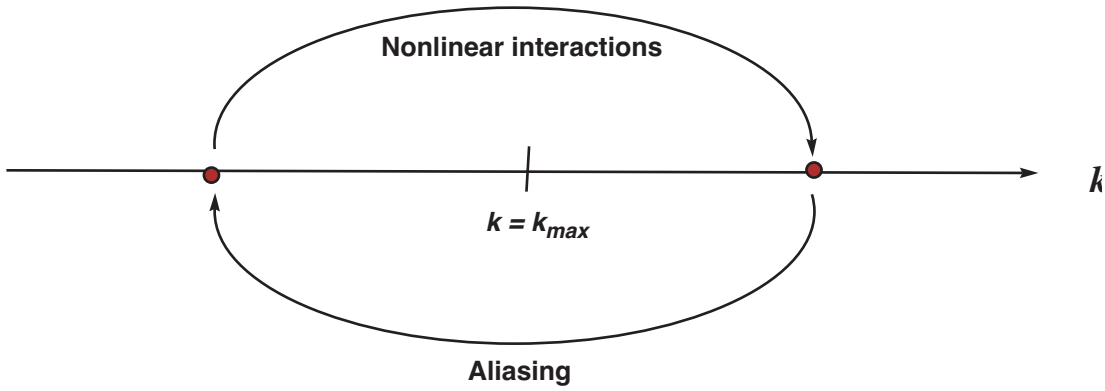

Figure 9.6: Schematic illustration of the mechanism of aliasing instability. Nonlinear interactions feed energy into scales too small to be represented on the grid, and this energy folds back through aliasing into scales that *can* be represented. The process feeds on itself. This can cause the total amount of energy to increase, unless the scheme is energy conserving.

could not increase, and the instability would be prevented, even though aliasing would still occur, and even though the truncation errors for the smallest scales would still be large. In the example, we used J_1. Later we demonstrate that J_1 does not conserve kinetic energy. Some other finite-difference Jacobians do conserve kinetic energy. Further discussion is given later.

Some further general insight into this type of instability (the above example being a

contrived special case) can be obtained by investigating the truncation error of the expression on the right side of (9.25). This can be expressed as

$$\frac{\partial q}{\partial t} = J_1(q,\psi) = J(q,\psi) + \frac{d^2}{6}\left[\frac{\partial q}{\partial x}\frac{\partial^3 \psi}{\partial y^3} - \frac{\partial q}{\partial y}\frac{\partial^3 \psi}{\partial x^3} + \frac{\partial^3 q}{\partial x^3}\frac{\partial \psi}{\partial y} - \frac{\partial^3 q}{\partial y^3}\frac{\partial \psi}{\partial x}\right] + O(d^4) \ . \quad (9.39)$$

Note the second-order accuracy. Through repeated integration by parts, it can be shown (after a page or so of algebra) that the second-order part of the truncation error in (9.39) is given by

$$\frac{d^2}{6}\int q\left[\frac{\partial q}{\partial x}\frac{\partial^3 \psi}{\partial y^3} - \frac{\partial q}{\partial y}\frac{\partial^3 \psi}{\partial x^3} + \frac{\partial^3 q}{\partial x^3}\frac{\partial \psi}{\partial y} - \frac{\partial^3 q}{\partial y^3}\frac{\partial \psi}{\partial x}\right] ds = \frac{d^2}{4}\int \frac{\partial^2 \psi}{\partial x \partial y}\left[\left(\frac{\partial q}{\partial x}\right)^2 - \left(\frac{\partial q}{\partial y}\right)^2\right] ds \ , \quad (9.40)$$

if q and its derivatives vanish at the boundary or if the domain is periodic. Multiplying (9.39) by q, integrating over the whole domain, and making use of (9.22), (9.23) and (9.40), we find that when we use J_1,

$$\frac{1}{2}\frac{\partial}{\partial t}\int q^2 ds = \frac{d^2}{4}\int \frac{\partial^2 \psi}{\partial x \partial y}\left[\left(\frac{\partial q}{\partial x}\right)^2 - \left(\frac{\partial q}{\partial y}\right)^2\right] ds + \int O(d^4) ds \ . \quad (9.41)$$

This means that, if $\frac{\partial^2 \psi}{\partial x \partial y} > 0$, q^2 will falsely grow with time if $\left(\frac{\partial q}{\partial x}\right)^2$ is bigger than $\left(\frac{\partial q}{\partial y}\right)^2$, in an overall sense. Now look at Fig. 9.7. In the figure, the streamlines are given such that $\psi_1 < \psi_2 < \psi_3$, so that $\partial \psi / \partial y < 0$, and $\frac{\partial^2 \psi}{\partial x \partial y} > 0$. This resembles the "exit" region of the jet stream. [Note: The stream function sketched in Fig. 9.7 does *not* correspond to (9.27).]

In fact, the solution of the differential-difference equation tends to prefer a positive value of the integrand of the right-hand side of (9.41), as illustrated schematically in Fig. 9.7. Notice that at t_2, $\frac{\partial q}{\partial x}$ becomes greater than it was at t_1, and the reverse is true for $\frac{\partial q}{\partial y}$. Therefore, although at t_1 the expression $\int \frac{\partial^2 \psi}{\partial x \partial y}\left[\left(\frac{\partial q}{\partial x}\right)^2 - \left(\frac{\partial q}{\partial y}\right)^2\right] ds$ vanishes, at t_2 it has become positive. From (9.41), it can be seen that the area-integrated q^2 tends to increase with time, whereas it is invariant in the differential case.

Aliasing instability has nothing to do with time truncation error. Making the time step shorter cannot prevent the instability, which can occur, in fact, even in the time-continuous case. The example we have just considered illustrates this fact, because we have left the time derivatives in continuous form.

A number of methods have been proposed to prevent or control aliasing instability.

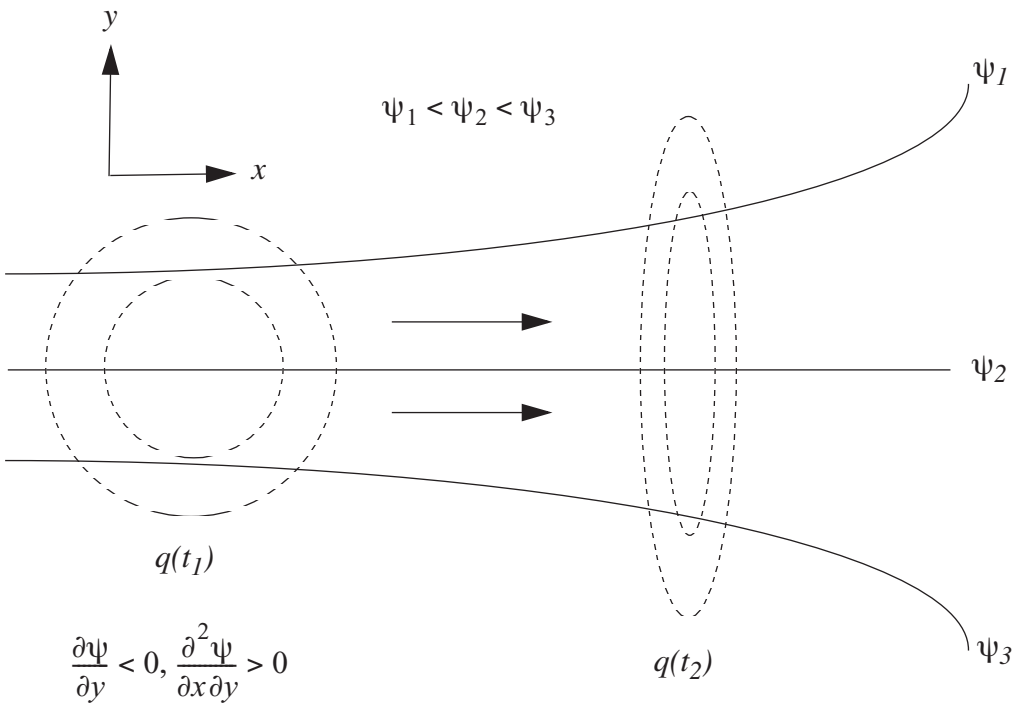

Figure 9.7: Sketch illustrating the mechanism of aliasing instability.

One method is to prevent aliasing. Aliasing error can actually be eliminated in a spectral model, at least for models that contain only "quadratic" aliasing, i.e., aliasing that arises from the multiplication of two spatially varying fields; this will be discussed later.

Phillips (1959) suggested that aliasing instability can be prevented if a Fourier analysis of the predicted fields is made after each time step, and all waves of wave number $k > \frac{k_{max}}{2}$ are simply discarded. With this "filtering" method, Phillips could guarantee absolutely no aliasing error due to quadratic nonlinearities, because the shortest possible wave would have wave number $\frac{k_{max}}{2}$ (his maximum wave number) and thus any wave generated by quadratic nonlinearities would have a wave number of at most k_{max}. This method is strongly dissipative, however.

Others have suggested that use of a dissipative scheme, such as the Lax-Wendroff scheme, can overcome aliasing instability. Experience shows that this is not true. The damping of a dissipative scheme depends on the value of $\frac{c\Delta t}{\Delta x}$, but aliasing instability can occur even for $\frac{c\Delta t}{\Delta x} \to 0$.

A third approach is to use a sign-preserving advection scheme, as discussed in Chapter 4, and advocated by Smolarkeiwicz (1991).

A fourth approach is to use space-differencing schemes for the advection terms that designed to conserve the square of the advected quantity. The "energy approach" to checking stability, discussed in Chapter 2, ensures that such schemes are computationally stable. This approach has the advantage that stability is ensured simply by mimicking a property of the exact equations.

To prevent aliasing instability with the momentum equations, we can use finite-difference schemes that conserve either kinetic energy, or enstrophy (squared vorticity), or both. This approach was developed by Arakawa (1966). It will be explained below, after a digression in which we discuss the nature of two-dimensional nondivergent flows.

9.3 Fjortoft's Theorem

In the absence of viscosity, *vorticity and enstrophy are both conserved in two-dimensional nondivergent flows*. The frictionless momentum equation for shallow water,

$$\frac{\partial \mathbf{v}}{\partial t} = -(\mathbf{v} \bullet \nabla)\mathbf{v} - f\mathbf{k} \times \mathbf{v} \ , \tag{9.42}$$

where

$$f \equiv 2\Omega \sin\varphi \tag{9.43}$$

is the coriolis parameter, Ω is the angular velocity of the Earth's rotation, and φ is latitude. By taking the curl of (9.45) we can obtain the vorticity equation

$$\frac{\partial \zeta}{\partial t} = -\mathbf{v} \bullet \nabla(\zeta + f) - (\zeta + f)\nabla \bullet \mathbf{v} \ . \tag{9.44}$$

When the flow is nondivergent, so that (9.7) is satisfied, the vorticity equation reduces to

$$\frac{\partial \zeta}{\partial t} = -\mathbf{v} \bullet \nabla(\zeta + f) \ , \tag{9.45}$$

Since f is independent of time, we can write (9.45) as

$$\frac{\partial}{\partial t}(\zeta + f) = -\mathbf{v} \bullet \nabla(\zeta + f) \ . \tag{9.46}$$

The says that the absolute vorticity is simply advected by the mean flow. We also see that only the sum $(\zeta + f)$ matters for the vorticity equation; henceforth we just replace $(\zeta + f)$ by ζ, for simplicity.

Using Eq. (9.8), we can show that the vorticity and the stream function are related by

$$\zeta \equiv \mathbf{k} \bullet (\nabla \times \mathbf{v}) = \nabla^2 \psi \,. \tag{9.47}$$

Eq. (9.45) can be rewritten as

$$\frac{\partial \zeta}{\partial t} = -\nabla \bullet (\mathbf{v}\zeta) \,, \tag{9.48}$$

or, alternatively, as

$$\frac{\partial \zeta}{\partial t} = J(\zeta, \psi) \,. \tag{9.49}$$

From (9.48) we see that the domain-averaged vorticity is conserved:

$$\frac{d}{dt}\bar{\zeta} = \overline{\frac{\partial \zeta}{\partial t}} = 0 \,. \tag{9.50}$$

By combining (9.49) and (9.21), we obtain

$$\overline{\zeta \frac{\partial \zeta}{\partial t}} = 0 \,, \tag{9.51}$$

from which it follows that the domain-average of the enstrophy is also conserved:

$$\frac{d}{dt}\left(\frac{1}{2}\overline{\zeta^2}\right) = 0 \,. \tag{9.52}$$

Similarly, from (9.49) and (9.20) we find that

$$\overline{\psi \frac{\partial \zeta}{\partial t}} = 0 \,. \tag{9.53}$$

To see what this implies, substitute (9.47) into (9.53), to obtain

$$\overline{\psi \frac{\partial}{\partial t} \nabla^2 \psi} = 0 \,. \tag{9.54}$$

This is equivalent to

$$
\begin{aligned}
0 &= \overline{\psi \frac{\partial}{\partial t} \nabla^2 \psi} \\
&= \overline{\psi \frac{\partial}{\partial t} [\nabla \cdot (\nabla \psi)]} \\
&= \overline{\psi \nabla \cdot \frac{\partial}{\partial t} \nabla \psi} \\
&= \overline{\nabla \cdot \left(\psi \frac{\partial}{\partial t} \nabla \psi \right)} - \overline{\nabla \psi \cdot \frac{\partial}{\partial t} \nabla \psi} \\
&= -\overline{\frac{\partial}{\partial t} \left(\frac{1}{2} |\nabla \psi|^2 \right)} .
\end{aligned}
\tag{9.55}
$$

Eq. (9.55) is a statement of kinetic energy conservation. We conclude that (9.53) implies kinetic energy conservation. In fact, we can show that

$$
\overline{K} = \overline{\psi \varsigma} . \tag{9.56}
$$

Since both kinetic energy and enstrophy are conserved in frictionless two-dimensional flows, their ratio is also conserved, and has the dimensions of a length squared:

$$
\frac{\text{energy}}{\text{enstrophy}} \sim \frac{L^2 t^{-2}}{t^{-2}} = L^2 . \tag{9.57}
$$

This length can be interpreted as the typical scale of energy-containing eddies, and (9.57) states that it is invariant. The implication is that energy does not cascade in frictionless two-dimensional flows; it "stays where it is" in wave number space.

The exchanges of energy and enstrophy among different scales in two-dimensional turbulence were studied by Fjortoft (1953), who obtained some very fundamental and famous results, which can be summarized in a simplified way as follows. Consider three equally

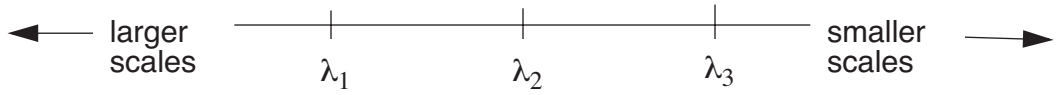

Figure 9.8: Diagram used in the explanation of Fjortoft's (1953) analysis of the exchanges of energy and enstrophy among differing scales in two-dimensional motion.

spaced wave numbers, as shown in Fig. 9.8. By "equally spaced" we mean that

$$
\lambda_2 - \lambda_1 = \lambda_3 - \lambda_2 = \Delta\lambda . \tag{9.58}
$$

The enstrophy, E, is

$$E = E_1 + E_2 + E_3 , \tag{9.59}$$

and the kinetic energy is

$$K = K_1 + K_2 + K_3 . \tag{9.60}$$

It can be shown that

$$E_n = \lambda_n^2 K_n , \tag{9.61}$$

where λ_n is a wave number, and the subscript n denotes a particular Fourier component. Suppose that kinetic energy is redistributed, i.e.

$$K_n \rightarrow K_n + \delta K_n , \tag{9.62}$$

such that

$$\sum \delta K_n = 0 , \tag{9.63}$$

$$\sum \delta E_n = 0 , \tag{9.64}$$

and note from (9.61) that

$$\delta E_n = \lambda_n^2 \delta K_n . \tag{9.65}$$

It follows that

$$\delta K_1 + \delta K_3 = -\delta K_2 , \tag{9.66}$$

$$\begin{aligned} \lambda_1^2 \delta K_1 + \lambda_3^2 \delta K_3 &= -\lambda_2^2 \delta K_2 \\ &= \lambda_2^2 (\delta K_1 + \delta K_3) . \end{aligned} \tag{9.67}$$

Collecting terms, we find that

$$\frac{\delta K_3}{\delta K_1} = \frac{\lambda_2^2 - \lambda_1^2}{\lambda_3^2 - \lambda_2^2} . \tag{9.68}$$

Using (9.58), we get

$$\frac{\delta K_3}{\delta K_1} = \frac{\lambda_2 + \lambda_1}{\lambda_3 + \lambda_2} < 1 \tag{9.69}$$

Eq. (9.69) shows that the energy transferred to higher wave numbers (δK_3) is less than the energy transferred to lower wave numbers (δK_1). This conclusion rests on both (9.63) and (9.64), i.e. on both energy conservation and enstrophy conservation. The implication is that kinetic energy actually "migrates" from higher wave numbers to lower wave numbers, i.e. from smaller scales to larger scales.

We now perform a similar analysis for the enstrophy. As a first step, we use (9.65) and (9.69) to write

$$\begin{aligned}\frac{\delta E_3}{\delta E_1} &= \frac{\lambda_3^2}{\lambda_1^2}\left(\frac{\lambda_2 + \lambda_1}{\lambda_3 + \lambda_2}\right) \\ &= \frac{(\lambda_2 + \Delta\lambda)^2\left(\lambda_2 - \frac{1}{2}\Delta\lambda\right)}{(\lambda_2 - \Delta\lambda)^2\left(\lambda_2 + \frac{1}{2}\Delta\lambda\right)} > 1.\end{aligned} \tag{9.70}$$

To show that this ratio is greater than one, we demonstrate that $\frac{\delta E_3}{\delta E_1} = a \cdot b \cdot c$, where a, b, and c are each greater than one. We can choose:

$$a = \frac{\lambda_2 + \Delta\lambda}{\lambda_2 - \Delta\lambda} > 1, \tag{9.71}$$

$$b = \frac{\lambda_2 - \frac{1}{2}\Delta\lambda}{\lambda_2 - \Delta\lambda} > 1, \tag{9.72}$$

$$c = \frac{\lambda_2 + \Delta\lambda}{\lambda_2 + \frac{1}{2}\Delta\lambda} > 1\ . \tag{9.73}$$

The conclusion is that enstrophy cascades to higher wave numbers in two-dimensional turbulence. Of course, such a cascade ultimately leads to enstrophy dissipation by viscosity.

The conclusion is that in two-dimensional turbulence, enstrophy is dissipated but kinetic energy is not.

In three-dimensions, vorticity is not conserved (nor is enstrophy) because of

stretching and twisting. Vortex stretching, in particular, causes small scales to gain energy at the expense of larger scales. As a result, kinetic energy cascades in three-dimensional turbulence. Ultimately the energy is converted from kinetic to internal by the viscous force.

In summary, vorticity and enstrophy are conserved in two-dimensional flow but not in three-dimensional flow. Kinetic energy is conserved under inertial processes in both two-dimensional and three-dimensional flows. Because two-dimensional flows are obliged to conserve both energy and enstrophy, they "have fewer options" than do three-dimensional flows. In particular, a kinetic energy cascade cannot happen in two-dimensions. What happens instead is an enstrophy cascade. Enstrophy is dissipated but kinetic energy is (almost) not.

Because kinetic energy does not cascade in two-dimensional flow, the motion remains smooth and is dominated by "large" eddies. This is true with the continuous equations, and we want it to be true in our models as well.

9.4 Kinetic energy and enstrophy conservation in two-dimensional non-divergent flow

Lorenz (1960) suggested that energy-conserving finite-difference schemes would be advantageous in efforts to produce realistic numerical simulations of the general circulation of the atmosphere. Arakawa (1966) developed a method for numerical simulation of two-dimensional, purely rotational motion, that conserves both kinetic energy and enstrophy. His method has been very widely used. The following is a summary of Arakawa's approach.

We begin by writing down a spatially discrete version of (9.49), keeping the time derivative in continuous form:

$$\begin{aligned} \sigma_{\boldsymbol{i}} \frac{d\zeta_{\boldsymbol{i}}}{dt} &= \sigma_{\boldsymbol{i}} J_{\boldsymbol{i}}(\zeta, \psi) \\ &= \sum_{\boldsymbol{i}'} \sum_{\boldsymbol{i}''} c_{\boldsymbol{i}, \boldsymbol{i}', \boldsymbol{i}''} \zeta_{\boldsymbol{i}+\boldsymbol{i}'} \psi_{\boldsymbol{i}+\boldsymbol{i}''} \, . \end{aligned} \tag{9.74}$$

Here the area of grid cell $\boldsymbol{i}$ is denoted by $\sigma_{\boldsymbol{i}}$. The bold subscripts are two-dimensional counters that can be used to specify a grid cell on a two-dimensional grid by giving a single number. For instance, we could start counting from the lower left corner of the grid, with $\boldsymbol{i} = 1$, and take the next grid point to the right as $\boldsymbol{i} = 2$, and so on, until we came to the end of the bottom row with $\boldsymbol{i} = I$, and then pick up at the left-most grid point of the second row from the bottom with $\boldsymbol{i} = I + 1$, etc. These two-dimensional counters are used to minimize the number of subscripts; we could use double subscripts (i, j) in the usual way, but choose not to just to keep the notation a little easier on the eyes. Just for reference, with double subscripts (9.74) would become

$$\sigma_{i,j} \frac{d\zeta_{i,j}}{dt} = \sum_{j'} \sum_{i'} \sum_{j''} \sum_{i''} c_{i,j;i',j';i'',j''} \zeta_{i',j'} \psi_{i'',j''} \, . \tag{9.75}$$

The second line of (9.74) looks a little mysterious and requires some explanation. As can be seen by inspection of (9.16), the Jacobian operator $J(\zeta, \psi)$ involves derivatives of the vorticity, multiplied by derivatives of the stream function. We can anticipate, therefore, that

the form we choose for the finite-difference Jacobian at the point $\boldsymbol{i}$ will involve products of the vorticity at some nearby grid points with the stream function at other nearby grid points. We have already seen an example of this in (9.25). Such products appear in (9.74). The neighboring grid points can be specified in (9.74) by assigning appropriate values to $\boldsymbol{i}'$ and $\boldsymbol{i}''$. The $c_{\boldsymbol{i},\boldsymbol{i}',\boldsymbol{i}''}$ are suitable "interaction coefficients" involving the grid distances, etc., and their form will be chosen later. It is by appropriate choices of the $c_{\boldsymbol{i},\boldsymbol{i}',\boldsymbol{i}''}$ that we will construct an approximation to the Jacobian. The double sum in (9.74) essentially picks out the combinations of ζ and ψ, at neighboring grid points, that we wish to bring into our finite-difference operator.

Of course, there is nothing about the form of (9.74) that shows that it is actually a consistent finite-difference approximation to the Jacobian operator; all we can say at this point is that (9.74) has the *potential* to be a consistent finite-difference approximation to the Jacobian operator, if we choose the interaction coefficients properly. We return to this point later. We note, however, that in order to ensure conservation of vorticity under advection, we must require that our finite-difference Jacobian satisfy

$$\begin{aligned} 0 &= \sum_{\boldsymbol{i}} \sigma_{\boldsymbol{i}} J_{\boldsymbol{i}}(\zeta, \psi) \\ &= \sum_{\boldsymbol{i}} \sum_{\boldsymbol{i}'} \sum_{\boldsymbol{i}''} c_{\boldsymbol{i},\boldsymbol{i}',\boldsymbol{i}''} \zeta_{\boldsymbol{i}+\boldsymbol{i}'} \psi_{\boldsymbol{i}+\boldsymbol{i}''} \quad . \end{aligned} \tag{9.76}$$

Another interesting and important point is that the form of (9.74) is so general that it is impossible to tell what kind of grid we are on. It could be a rectangular grid on a plane, or a latitude-longitude grid on the sphere, or something more exotic like a geodesic grid on the sphere (to be discussed later).

Before going on, let's consider an example. Recall that in (9.25) we have already introduced a finite-difference Jacobian called J_1, which is defined on a square grid. We can write

$$\begin{aligned} &[J_1(\zeta, \psi)]_{i,j} \equiv \\ &\frac{1}{4d^2}[(\zeta_{i+1,j} - \zeta_{i-1,j})(\psi_{i,j+1} - \psi_{i,j-1}) - (\zeta_{i,j+1} - \zeta_{i,j-1})(\psi_{i+1,j} - \psi_{i-1,j})] \quad . \end{aligned} \tag{9.77}$$

Expanding, and using $\sigma_{i,j} = d^2$, we find that

$$\begin{aligned} &\sigma_{i,j}[J_1(\zeta, \psi)]_{i,j} \equiv \\ &\frac{1}{4}(\zeta_{i+1,j}\psi_{i,j+1} - \zeta_{i+1,j}\psi_{i,j-1} - \zeta_{i-1,j}\psi_{i,j+1} + \zeta_{i-1,j}\psi_{i,j-1} \\ &- \zeta_{i,j+1}\psi_{i+1,j} + \zeta_{i,j+1}\psi_{i-1,j} + \zeta_{i,j-1}\psi_{i+1,j} - \zeta_{i,j-1}\psi_{i-1,j}) \quad . \end{aligned} \tag{9.78}$$

Comparing (9.78) with (9.74), we identify

$$
\begin{aligned}
c_{i,j;i+1,j;i,j+1} &= \frac{1}{4} \ , \\
c_{i,j;i+1,j;i,j-1} &= -\frac{1}{4} \ , \\
c_{i,j;i-1,j;i,j+1} &= -\frac{1}{4} \ , \\
c_{i,j;i-1,j;i,j-1} &= \frac{1}{4} \ , \\
c_{i,j;i,j+1;i+1,j} &= -\frac{1}{4} \ , \\
c_{i,j;i,j+1;i-1,j} &= \frac{1}{4} \ , \\
c_{i,j;i,j-1;i+1,j} &= \frac{1}{4} \ , \\
c_{i,j;i,j-1;i-1,j} &= -\frac{1}{4} \ .
\end{aligned}
\tag{9.79}
$$

Look carefully at the subscripts. It should be clear that $c_{i,j;i+1,j;i,j+1}$ specifies contributions of the vorticity east of the point (i,j) and the stream function north of the point (i,j) to the time rate of change of the vorticity at the point i,j. In this simple case of a uniform square grid, the coefficients are very simple. Exactly the same formalism can be applied to much more complicated cases, however, such as nonuniform grids on a sphere.

Is (9.76) satisfied for J_1? Each term of the triple sum in (9.76) involves the product of a vorticity and a stream function. Each product will appear exactly twice when we form the sum. In order for (9.76) to be satisfied for arbitrary values of the vorticity and the stream function, we need the two contributions from each product to cancel in the sum, i.e., their coefficients must be equal and opposite. As pointed out above, $c_{i,j;i+1,j;i,j+1}$ specifies the contributions of the vorticity at $i+1,j$ and the stream function at $i,j+1$ to the time rate of change of the vorticity at the point i,j. Similarly, $c_{i+1,j+1;i+1,j;i,j+1}$ specifies the contributions of the vorticity at $i+1,j$ and the stream function at $i,j+1$ to the time rate of change of the vorticity at the point $i+1,j+1$. See Fig. 9.9. Cancellation will occur if

$$
c_{i,j;i+1,j;i,j+1} = -c_{i+1,j+1;i+1,j;i,j+1} \ . \tag{9.80}
$$

To see whether or not this is the case, note that the value of $c_{i+1,j+1;i+1,j;i,j+1}$ must remain unchanged if we subtract one from each i subscript and one from each j subscript. In other words,

$$
c_{i+1,j+1;i+1,j;i,j+1} = c_{i,j;i,j-1;i-1,j} \ . \tag{9.81}
$$

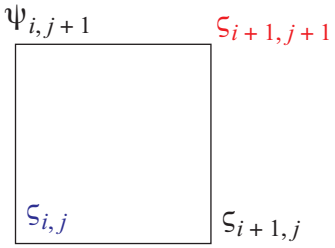

Figure 9.9: Stencil used in the discussion of vorticity conservation for J_1. See text for details.

Therefore the requirement (9.80) is equivalent to

$$c_{i,j;i+1,j;i,j+1} = -c_{i,j;i,j-1;i-1,j} . \tag{9.82}$$

What has been accomplished by subtracting one from each subscript is that in the result, i.e., (9.82), both of the cs are associated with the time-rate of change at the point (i,j), and so both of them are explicitly listed in (9.79). Inspection of (9.79) shows that (9.82) is indeed satisfied. Similar results apply for the remaining terms. In this way, we can prove that J_1 conserves vorticity.

Returning to the general problem, what we are going to do now is find a way to enforce finite-difference analogs of (9.51) and (9.53):

$$0 = \sum_i \sigma_i \zeta_i J_i(\zeta,\psi) = \sum_i \zeta_i \left(\sum_{i'} \sum_{i''} c_{i,i',i''} \zeta_{i+i'} \psi_{i+i''} \right) , \tag{9.83}$$

$$0 = \sum_i \sigma_i \psi_i J_i(\zeta,\psi) = \sum_i \psi_i \left(\sum_{i'} \sum_{i''} c_{i,i',i''} \zeta_{i+i'} \psi_{i+i''} \right) . \tag{9.84}$$

By enforcing these two requirements we can ensure conservation of enstrophy and kinetic energy in the finite-difference model. The requirements can be met, as we will see, by suitable choice of the interaction coefficients. The requirements look daunting, though, because they involve triple sums. How in the world are we ever going to work this out?

Inspection of (9.83) shows that the individual terms of the sum are going to involve products of vorticities at pairs of grid points. With this in mind, we go back to (9.74) and rewrite it as

$$\begin{aligned} \sigma_i J_i(\zeta,\psi) &= \sum_{i'} \sum_{i''} c_{i,i',i''} \zeta_{i+i'} \psi_{i+i''} \\ &= \sum_{i'} a_{i,i+i'} \zeta_{i+i'} \quad , \end{aligned} \tag{9.85}$$

where, by definition,

$$a_{i,\,i+i'} \equiv \sum_{i''} c_{i,\,i',\,i''}\psi_{i+i''} \,. \tag{9.86}$$

Multiply (9.85) by ζ_i to obtain

$$\sigma_i\zeta_i J_i(\zeta,\,\psi) \;=\; \sum_{i'} a_{i,\,i+i'}\zeta_i\zeta_{i+i'} \,. \tag{9.87}$$

Here we have simply taken ζ_i inside the sum, which we can do because the sum is over i', not i. From this point it is straightforward to enforce (9.83), which can be rewritten as

$$0 \;=\; \sum_{i}\left(\sum_{i'} a_{i,\,i+i'}\zeta_i\zeta_{i+i'}\right) . \tag{9.88}$$

Think of the outer sum in (9.88) as a "DO" loop. As we sweep over the grid, each product $\zeta_i\zeta_{i+i'}$ will enter the sum exactly twice. We can specify the vorticities any way we want, e.g., when we set up the initial conditions, so the only way to make sure that (9.88) is satisfied is to force these two contributions to the sum to be equal and opposite, i.e. we must take

$$a_{i,\,i+i'} \;=\; -a_{i+i',\,i}\,, \text{ for all } i \text{ and } i' \,. \tag{9.89}$$

By enforcing (9.89), we can ensure enstrophy conservation.

Kinetic energy conservation can be guaranteed by a very similar approach. We rewrite (9.74) as

$$\begin{aligned} \sigma_i J_i(\zeta,\,\psi) \;&=\; \sum_{i'}\sum_{i''} c_{i,\,i',\,i''}\zeta_{i+i'}\psi_{i+i''} \\ &=\; \sum_{i''} b_{i,\,i+i''}\psi_{i+i''} \;\;, \end{aligned} \tag{9.90}$$

where

$$b_{i,\,i+i''} \equiv \sum_{i'} c_{i,\,i',\,i''}\zeta_{i+i'} \,. \tag{9.91}$$

By an argument similar to that given above, we find that

$$b_{i,\,i+i''} \;=\; -b_{i+i'',\,i} \text{ for all } i \text{ and } i' \tag{9.92}$$

is necessary to ensure kinetic energy conservation.

As already mentioned, we have not assumed anything about the shape of the domain.

It could be a doubly periodic plane, or it could be a sphere. Also, we have not assumed anything about the grid. The individual cells have not been assumed to have any particular shape, e.g. quadrilaterals; the argument starting from (9.74) would apply equally well on a grid of hexagons.

At this point we acknowledge that (9.92) is not really sufficient to ensure kinetic energy conservation. We must also make sure that the finite-difference analog of (9.55) holds true, i.e.

$$\sum_i \left(\sigma_i \psi_i \frac{d\zeta_i}{dt} \right) = -\sum_i \left[\sigma_i \frac{d}{dt} \left(\frac{1}{2} |\nabla \psi|_i^2 \right) \right], \tag{9.93}$$

so that we can mimic with the finite-difference equations the derivation that we did with the continuous equations. In order to pursue this objective, we have to define a finite-difference Laplacian, and we do so now by choosing the simplest possibility, assuming a square grid with grid spacing d:

$$\zeta_{i,j} = (\nabla^2 \psi)_{i,j} \equiv \frac{1}{d^2} (\psi_{i+1,j} + \psi_{i-1,j} + \psi_{i,j+1} + \psi_{i,j-1} - 4\psi_{i,j}) \ . \tag{9.94}$$

Here we have reverted to a conventional double-subscripting scheme, for clarity. We also define a finite-difference kinetic energy by

$$\begin{aligned} K_{i,j} &= \frac{1}{2} |\nabla \psi|_{i,j}^2 \\ &\equiv \frac{1}{4d^2} [(\psi_{i+1,j} - \psi_{i,j})^2 + (\psi_{i,j+1} - \psi_{i,j})^2 + (\psi_{i,j} - \psi_{i-1,j})^2 + (\psi_{i,j} - \psi_{i,j-1})^2] \end{aligned} \tag{9.95}$$

Because the right-hand side of (9.95) is a sum of squares, we are guaranteed that the kinetic energy is non-negative. By substitution, and after a little algebra, we can show that (9.94) and (9.95) do, in fact, satisfy (9.93).

This is all fine, as far as it goes, but we still have some very basic and important business to attend to: We have not yet ensured that the sum in (9.74) is actually a consistent finite-difference approximation to the Jacobian operator. The approach that we will follow is to write down three independent finite-difference Jacobians and then identify, by inspection, the c's in (9.74). When we say that the Jacobians are "independent" we mean that it is not possible to write any one of the three as a linear combination of the other two. The three finite-difference Jacobians are:

$$\begin{aligned} (J_1)_{i,j} = \frac{1}{4d^2} [&(\zeta_{i+1,j} - \zeta_{i-1,j})(\psi_{i,j+1} - \psi_{i,j-1}) \\ &-(\zeta_{i,j+1} - \zeta_{i,j-1})(\psi_{i+1,j} - \psi_{i-1,j})], \end{aligned} \tag{9.96}$$

$$(J_2)_{i,j} = \frac{1}{4d^2}[-(\zeta_{i+1,j+1} - \zeta_{i+1,j-1})\psi_{i+1,j} + (\zeta_{i-1,j+1} - \zeta_{i-1,j-1})\psi_{i-1,j} + (\zeta_{i+1,j+1} - \zeta_{i-1,j+1})\psi_{i,j+1} - (\zeta_{i+1,j-1} - \zeta_{i-1,j-1})\psi_{i,j-1}], \tag{9.97}$$

$$(J_3)_{i,j} = \frac{1}{4d^2}[\zeta_{i+1,j}(\psi_{i+1,j+1} - \psi_{i+1,j-1}) - \zeta_{i-1,j}(\psi_{i-1,j+1} - \psi_{i-1,j-1}) - \zeta_{i,j+1}(\psi_{i+1,j+1} - \psi_{i-1,j+1}) + \zeta_{i,j-1}(\psi_{i+1,j-1} - \psi_{i-1,j-1})]. \tag{9.98}$$

These can be interpreted, respectively, as finite-difference analogs to the right-hand sides of (9.16) - (9.18). We can show that all three of these finite-difference Jacobians are consistent with vorticity conservation under advection, i.e., they all satisfy (9.76).

What we need to do next is identify the coefficients a and b for each of (9.96), (9.97), and (9.98), and then check to see whether the requirements (9.89) and (9.92) are satisfied for any of them. In order to understand more clearly what these requirements actually mean, look at Fig. 9.10. The Jacobians J_1, J_2, and J_3 are represented in the top row of the figure. The

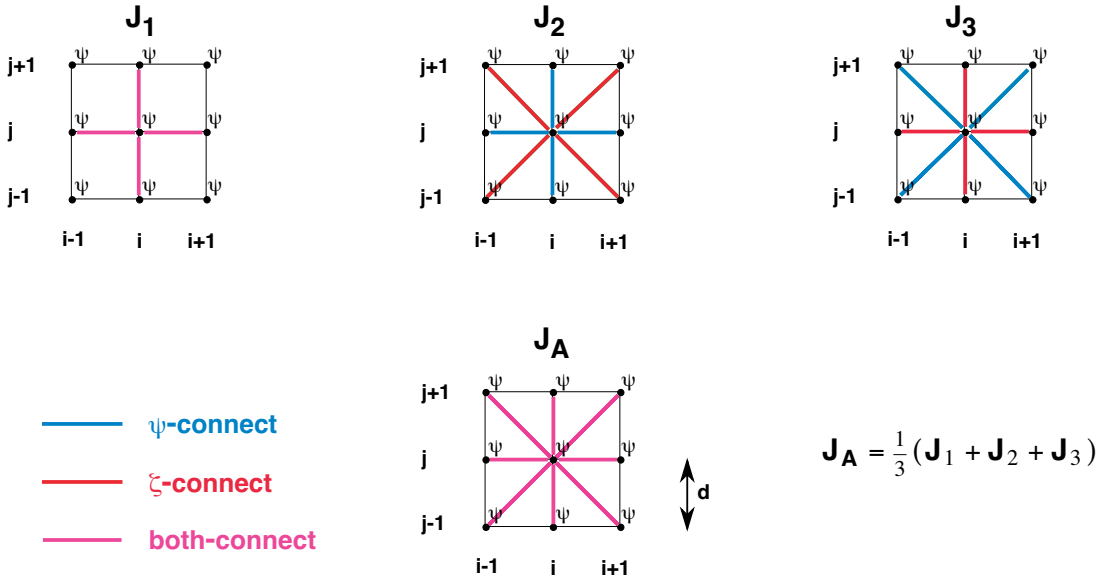

Figure 9.10: The central point in each figure is (i,j). Stream function and vorticity are both defined at each of the mesh points indicated by the black dots. The colored lines represent contributions to $J_{i,j}$ from ψ, ζ, or both, from the various neighboring points.

colored lines show how each Jacobian at the point (i,j) is influenced (or not) by the stream

function and vorticity at the various neighboring points. We begin by rewriting (9.85) using the conventional double-subscript notation and equating it to $(J_1)_{i,j}$:

$$\begin{aligned}\sigma_{i,j}(J_1)_{i,j}(\zeta,\psi) &= \sum_{i'}\sum_{j'}\sum_{i''}\sum_{j''} c_{i',j';i'',j''}\,\zeta_{i,j;i+i',j+j'}\psi_{i+i'',j+j''} \\ &= \sum_{i'}\sum_{j'} a_{i,j;i+i',j+j'}\zeta_{i,j;i+i',j+j'} \\ &= \frac{1}{4}[(\zeta_{i+1,j}-\zeta_{i-1,j})(\psi_{i,j+1}-\psi_{i,j-1})-(\zeta_{i,j+1}-\zeta_{i,j-1})(\psi_{i+1,j}-\psi_{i-1,j})] \\ &= \frac{1}{4}[\zeta_{i+1,j}(\psi_{i,j+1}-\psi_{i,j-1})-\zeta_{i-1,j}(\psi_{i,j+1}-\psi_{i,j-1}) \\ &\quad -\zeta_{i,j+1}(\psi_{i+1,j}-\psi_{i-1,j})+\zeta_{i,j-1}(\psi_{i+1,j}-\psi_{i-1,j})].\end{aligned} \tag{9.99}$$

Here we have used

$$\sigma_{i,j} = d^2 . \tag{9.100}$$

By inspection of (9.99) and comparison with (9.85), we can read off the definitions of the a coefficients for J_1:

$$a_{i,j;i+1,j} = \frac{1}{4}(\psi_{i,j+1}-\psi_{i,j-1}) , \tag{9.101}$$

$$a_{i,j;i-1,j} = -\frac{1}{4}(\psi_{i,j+1}-\psi_{i,j-1}) , \tag{9.102}$$

$$a_{i,j;i,j+1} = -\frac{1}{4}(\psi_{i+1,j}-\psi_{i-1,j}) , \tag{9.103}$$

$$a_{i,j;i,j-1} = \frac{1}{4}(\psi_{i+1,j}-\psi_{i-1,j}) . \tag{9.104}$$

Are these consistent with (9.89)? To find out, replace i by $i+1$ in (9.102); this gives:

$$a_{i+1,j;i,j} = -\frac{1}{4}(\psi_{i+1,j+1}-\psi_{i+1,j-1}) . \tag{9.105}$$

Now simply compare (9.105) with (9.101), to see that (9.89) is *not* satisfied by J_1. We have thus deduced that J_1 does not conserve enstrophy.

We can interpret that $a_{\boldsymbol{i},\,\boldsymbol{i}+\boldsymbol{i}'}$ denotes ζ-interactions of point $\boldsymbol{i}$ with point $\boldsymbol{i}+\boldsymbol{i}'$, while $a_{\boldsymbol{i}+\boldsymbol{i}',\,\boldsymbol{i}}$ denotes ζ-interactions of point $\boldsymbol{i}+\boldsymbol{i}'$ with point $\boldsymbol{i}$. When we compare $a_{\boldsymbol{i},\,\boldsymbol{i}+\boldsymbol{i}'}$ with $a_{\boldsymbol{i}+\boldsymbol{i}',\,\boldsymbol{i}}$, it is like peering along one of the red lines in Fig. 9.10, first outward from the point (i,j), to one of the other points, and then back towards the point (i,j). The condition (9.89) on the a's essentially means that all such interactions are "equal and opposite," allowing suitable algebraic cancellations to occur when we sum over all points. The condition (9.92) on the b's has a similar interpretation.

By proceeding as illustrated above, we can reach the following conclusions:

- J_1 conserves neither enstrophy nor kinetic energy;
- J_2 conserves enstrophy but not kinetic energy; and
- J_3 conserves kinetic energy but not enstrophy.

It looks like we are out of luck.

We can form a new Jacobian, however, by combining J_1, J_2, and J_3 with weights, as follows:

$$J_A = \alpha J_1 + \beta J_2 + \gamma J_3 , \tag{9.106}$$

such that

$$\alpha + \beta + \gamma = 1 . \tag{9.107}$$

With three unknown coefficients, and only one constraint, (9.107), we are free to satisfy two additional constraints; and we take these to be (9.89) and (9.92). In this way, we find that J_A will conserve both enstrophy and kinetic energy if we choose

$$\alpha = \beta = \gamma = 1/3 . \tag{9.108}$$

The composite Jacobian J_A is often called the "Arakawa Jacobian."

Fig. 9.11 shows the results of tests with J_1, J_2, and J_3, and also with three other Jacobians called J_4, J_5, and J_6, as well as with J_A. The leapfrog time-differencing scheme was used in these tests; the influence of time differencing on the conservation properties of the schemes will be discussed later; it is minor, so long as we do not violate the criteria for linear computational instability. The various space-differencing schemes do indeed display the conservation properties expected on the basis of the preceding analysis.

The approach outlined above yields a conservative second-order accurate (in space) finite-difference approximation to the Jacobian. Arakawa (1966) also showed how to obtain

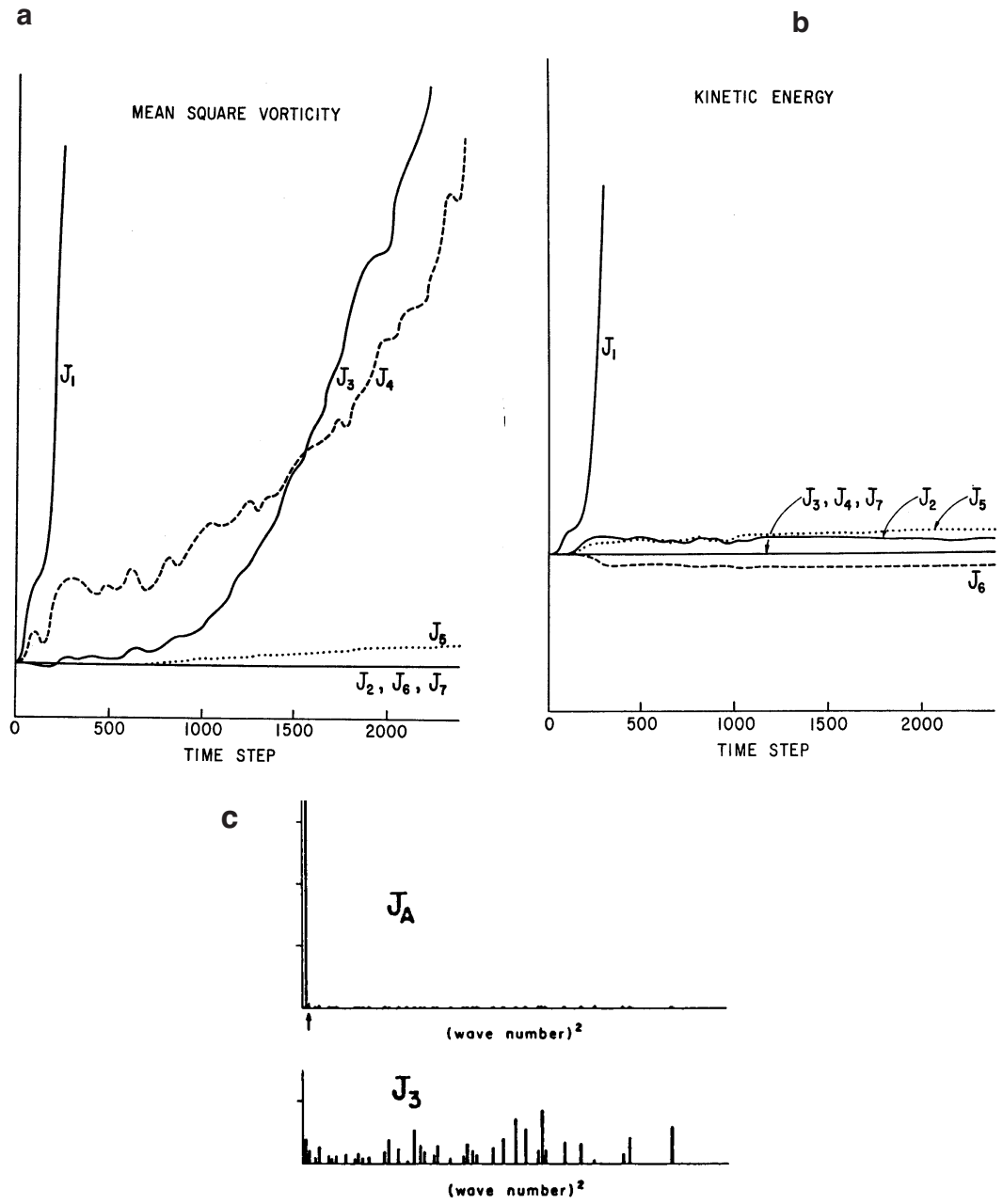

Figure 9.11: Results of tests with the various finite-difference Jacobians. Panel c shows the initial kinetic energy is at a low wave number.

the corresponding conservative Jacobian with fourth-order accuracy.

The preceding analysis shows how vorticity, kinetic energy and enstrophy can be conserved under advection in numerical simulations of two-dimensional non-divergent flow. In practice, however, we have to consider the presence of divergence. When the flow is divergent, vorticity and enstrophy are not conserved, but potential vorticity and potential

enstrophy are conserved.

In Chapter 4, we concluded that, by suitable choice of the interpolated "cell-wall" values of an arbitrary advected quantity, A, it is possible to conserve exactly one non-trivial function of A, i.e. $F(A)$, in addition to A itself. Conserving more than A and one $F(A)$ was not possible because the only freedom that we had to work with was the form of the interpolated "cell-wall" value, which was denoted by $\hat{A}$. Once we chose $\hat{A}$ so as to conserve, say, A^2, we had no room left to maneuver, so we could not conserve anything else. We have just shown, however, that the vorticity equation for two-dimensional nondivergent flow can be discretized so as to conserve two quantities, namely the kinetic energy and the enstrophy, in addition to the vorticity itself. What is going on?

The key difference with the vorticity equation is that we can choose not only how to interpolate the vorticity (so as to conserve the enstrophy), but also *the actual finite-difference expression for the advecting wind itself*, in terms of the stream function, because that expression is implicit in the form of the Jacobian that we use. In choosing the form of the advecting current, we have a second "freedom," which allows us to conserve a second quantity, namely the kinetic energy.

As discussed earlier, the constraint of enstrophy conservation is needed to ensure that kinetic energy does not cascade in two-dimensional nondivergent flow. If kinetic energy does not cascade, the flow remains smooth. When the flow is smooth, kinetic energy conservation is approximately satisfied, even if it is not exactly guaranteed by the scheme. This means that a scheme that exactly conserves enstrophy and approximately conserves kinetic energy will behave well.

In contrast, a scheme that conserves kinetic energy but not enstrophy will permit a kinetic energy cascade. The resulting noisy flow will lead to large errors in enstrophy conservation. Such a scheme will not behave well.

These considerations suggest that formal enstrophy conservation is "more important" than formal kinetic energy conservation.

9.5 Angular momentum conservation

Finally, for completeness, define the relative angular momentum per unit mass, M, by

$$M_{\text{rel}} \equiv ua\cos\varphi \,. \tag{9.109}$$

This is actually the component of the relative angular momentum vector in the direction of the axis of the Earth's rotation. Here we consider motion on the sphere, a is the radius of the Earth, and u is the zonal component of the wind. From the momentum equation we can show that in the absence of pressure-gradient forces and friction,

$$\frac{\partial M}{\partial t} = -(\mathbf{v} \bullet \nabla)M \,, \tag{9.110}$$

where λ is longitude, and

$$M \equiv M_{\text{rel}} + \Omega a^2 \cos\varphi \tag{9.111}$$

is the component of the absolute angular momentum vector in the direction of the axis of the Earth's rotation. From (9.110) it follows that the absolute angular momentum is conserved under advection.

Using integration by parts, it can be demonstrated that

$$\overline{M_{\text{rel}}} = a^2 \int_{-\frac{\pi}{2}}^{\frac{\pi}{2}} \int_0^{2\pi} (\sin\varphi)\zeta \cos\varphi \; d\lambda d\varphi \,. \tag{9.112}$$

We can also prove that

$$\frac{d}{dt}\overline{M_{\text{rel}}} = a^2 \int_{-\frac{\pi}{2}}^{\frac{\pi}{2}} \int_0^{2\pi} (\sin\varphi)\frac{\partial \zeta}{\partial t} \cos\varphi \; d\lambda d\varphi = 0 \,. \tag{9.113}$$

This means that angular momentum is conserved.

9.6 Conservative schemes for the two-dimensional shallow water equations with rotation

To study the two-dimensional shallow-water equations, we use cartesian coordinates x and y, with velocity vector $\mathbf{V}$, such that

$$\mathbf{V} \equiv u\mathbf{i} + v\mathbf{j} \,, \tag{9.114}$$

where $\mathbf{i}$ and $\mathbf{j}$ are the unit vectors in the x and y directions, respectively. The shallow-water equations can be written as

$$\frac{\partial h}{\partial t} + \nabla\bullet(h\mathbf{V}) = 0 \,, \tag{9.115}$$

and

$$\frac{\partial \mathbf{V}}{\partial t} + \left(\frac{\zeta + f}{h}\right)\mathbf{k} \times (h\mathbf{V}) + \nabla[K + g(h + h_S)] = 0 \quad , \tag{9.116}$$

where

$$\zeta \equiv \mathbf{k} \bullet (\nabla \times \mathbf{V}) \tag{9.117}$$

is the relative vorticity, and

$$f \equiv 2\Omega \sin\varphi \tag{9.118}$$

is the Coriolis parameter. In (9.116), we have multiplied and divided the vorticity term by h, for two good reasons, to be explained later. The combination $\left(\frac{\zeta + f}{h}\right)$ is the potential vorticity.

The corresponding equations for the zonal and meridional wind components are

$$\frac{\partial u}{\partial t} - \left(\frac{\zeta + f}{h}\right)(hv) + \frac{\partial}{\partial x}[K + g(h + h_S)] = 0 \quad , \tag{9.119}$$

and

$$\frac{\partial v}{\partial t} + \left(\frac{\zeta + f}{h}\right)(hu) + \frac{\partial}{\partial y}[K + g(h + h_S)] = 0 \ , \tag{9.120}$$

respectively.

When we take the dot product of (9.116) with $h\mathbf{V}$, the vorticity term of (9.116) contributes nothing because of the vector identity

$$(h\mathbf{V}) \bullet [\mathbf{k} \times (h\mathbf{V})] = 0 \ , \tag{9.121}$$

and so we obtain very directly the advective form of the kinetic energy equation, i.e.

$$h\frac{\partial K}{\partial t} + (h\mathbf{V}) \bullet \nabla[K + g(h + h_S)] = 0 \, , \tag{9.122}$$

where $K \equiv \frac{1}{2}\mathbf{V} \bullet \mathbf{V}$ is the kinetic energy per unit mass. By use of the continuity equation (9.115), we can rewrite (9.122) in flux form:

$$\frac{\partial}{\partial t}(hK) + \nabla\bullet(h\mathbf{V}K) + (h\mathbf{V}) \bullet \nabla[g(h + h_S)] = 0 \, . \tag{9.123}$$

Similarly, the flux form of the potential energy equation is

$$\frac{\partial}{\partial t}\left[h\left(gh_S + \frac{1}{2}h\right)\right] + \nabla\bullet[(h\mathbf{V})g(h + h_S)] - (h\mathbf{V}) \bullet \nabla[g(h + h_S)] = 0 \, . \tag{9.124}$$

The method presented earlier to ensure conservation of kinetic energy for the one-dimensional finite-difference shallow-water equations carries through to two dimensions in very straightforward fashion, and so the details will not be given here. The important new physical ingredient that must be considered in the two-dimensional finite-difference system is rotation. We have already considered the effects of rotation for the case of two-dimensional nondivergent flow. Now we have divergence, so in place of vorticity conservation and enstrophy conservation we must consider potential vorticity conservation and potential

enstrophy conservation. One obvious and important question is: *Can we find a finite-difference analog to (9.121)?*

The approach outlined below follows Arakawa and Lamb (1981). We adopt the C grid, as shown in Fig. 9.12. Recall that on the C grid the zonal winds are east and west of the

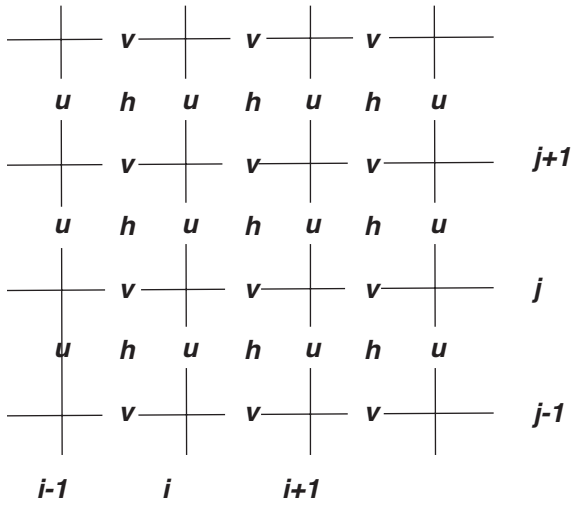

Figure 9.12: The arrangement of the mass, zonal wind, and meridional wind on the C grid.

mass points, and the meridional winds are north and south of the mass points. The divergence "wants" to be defined at mass points, e.g. at point (i, j); and the vorticity "wants" to be defined along the diagonal lines connecting mass points, e.g., at the point $(i + 1/2, j - 1/2)$.

The finite-difference form of the continuity equation is

$$\frac{dh_{i+\frac{1}{2},j+\frac{1}{2}}}{dt} = \frac{(hu)_{i,j+\frac{1}{2}} - (hu)_{i+1,j+\frac{1}{2}}}{\Delta x} + \frac{(hv)_{i+\frac{1}{2},j} - (hv)_{i+\frac{1}{2},j+1}}{\Delta y} . \tag{9.125}$$

The various mass fluxes that appear in (9.125) have not yet been defined, but mass will be conserved regardless of how we define them.

Simple finite-difference analogs of the two components of the momentum equation are

$$\begin{aligned} &\frac{d}{dt}u_{i,j+\frac{1}{2}} - \left[\left(\frac{\zeta + f}{h}\right)(hv)\right]_{i,j+\frac{1}{2}} \\ &+ \frac{1}{\Delta x}\left(K_{i+\frac{1}{2},j+\frac{1}{2}} - K_{i-\frac{1}{2},j+\frac{1}{2}}\right) + \frac{g}{\Delta x}\left[(h + h_S)_{i+\frac{1}{2},j+\frac{1}{2}} - (h + h_S)_{i-\frac{1}{2},j+\frac{1}{2}}\right] = 0 , \end{aligned} \tag{9.126}$$

and

$$\frac{d}{dt}v_{i+\frac{1}{2},j} + \left[\left(\frac{\zeta+f}{h}\right)(hu)\right]_{i+\frac{1}{2},j} + \frac{1}{\Delta y}\left(K_{i+\frac{1}{2},j+\frac{1}{2}} - K_{i+\frac{1}{2},j-\frac{1}{2}}\right) + \frac{g}{\Delta y}\left[(h+h_S)_{i+\frac{1}{2},j+\frac{1}{2}} - (h+h_S)_{i+\frac{1}{2},j-\frac{1}{2}}\right] = 0\,, \tag{9.127}$$

respectively. As in the one-dimensional case, the kinetic energy per unit mass, $K_{i+\frac{1}{2},j+\frac{1}{2}}$, is undefined at this stage, but resides at mass points. The potential vorticities $\left(\frac{\zeta+f}{h}\right)_{i,j+\frac{1}{2}}$ and $\left(\frac{\zeta+f}{h}\right)_{i+\frac{1}{2},j}$, and the mass fluxes $(hv)_{i,j+\frac{1}{2}}$ and $(hu)_{i+\frac{1}{2},j}$ are also undefined.

Note that on the C-grid the mass fluxes that appear in (9.130) and (9.126) are in the "wrong" places; the mass flux $(hv)_{i,j+\frac{1}{2}}$ which appears in the equation for the *u*-wind is evidently at a *u*-wind point, and the mass flux $(hu)_{i+\frac{1}{2},j}$ which appears in the equation for the *v*-wind is evidently at a *v*-wind point. The vorticities that appear in (9.126) and (9.126) are also in the "wrong" places. Obviously, what we have to do is interpolate somehow to obtain mass fluxes and vorticities suitable for use in the vorticity terms of (9.126) and (9.126). Note, however, that it is actually *products* of mass fluxes and vorticities that are needed.

Arakawa and Lamb constructed the finite-difference vorticity terms in such a way that a finite-difference analog to (9.121) is satisfied, regardless of the specific forms of the mass fluxes and potential vorticities that are chosen. They constructed the vorticity terms as follows:

$$\left[\left(\frac{\zeta+f}{h}\right)(hv)\right]_{i,j+\frac{1}{2}} = \alpha_{i,j+\frac{1}{2};i+\frac{1}{2},j+1}(hv)_{i+\frac{1}{2},j+1} + \beta_{i,j+\frac{1}{2};i-\frac{1}{2},j+1}(hv)_{i-\frac{1}{2},j+1} + \gamma_{i,j+\frac{1}{2};i-\frac{1}{2},j}(hv)_{i-\frac{1}{2},j} + \delta_{i,j+\frac{1}{2};i+\frac{1}{2},j}(hv)_{i+\frac{1}{2},j}\,, \tag{9.128}$$

and

$$\left[\left(\frac{\zeta+f}{h}\right)(hu)\right]_{i+\frac{1}{2},j} = \gamma_{i+\frac{1}{2},j;i+1,j+\frac{1}{2}}(hu)_{i+1,j+\frac{1}{2}} + \delta_{i+\frac{1}{2},j;i,j+\frac{1}{2}}(hu)_{i,j+\frac{1}{2}} + \alpha_{i+\frac{1}{2},j;i,j-\frac{1}{2}}(hu)_{i,j-\frac{1}{2}} + \beta_{i+\frac{1}{2},j;i+1,j-\frac{1}{2}}(hu)_{i+1,j-\frac{1}{2}}\,. \tag{9.129}$$

In reality, the forms assumed by Arakawa and Lamb are slightly more general and slightly more complicated than these; we simplify here for ease of exposition. In (9.128) and (9.129), the α's, β's, γ's, and δ's obviously represent interpolated potential vorticities, whose forms are not yet specified. Each of these quantities has four subscripts, to indicate that it links a specific *u*-wind point with a specific *v*-wind point. The α's, β's, γ's, and δ's are somewhat analogous to the *a*'s and *b*'s that were defined in the discussion of two-dimensional non-divergent flow, in that the *a*'s and *b*'s also linked pairs of points. In (9.128), the interpolated potential vorticities multiply the mass fluxes hv at the four *v*-wind points surrounding the *u*-wind point $i, j + \frac{1}{2}$, and similarly in (9.129) they multiply the mass fluxes hu at the four *u*-wind points surrounding the *v*-wind point $i + \frac{1}{2}, j$.

When we form the kinetic energy equation, we have to take the dot product of the vector momentum equation with the mass flux $h\mathbf{V}$. This means that we have to multiply (9.126) by $(hu)_{i,j+\frac{1}{2}}$ and (9.126) by $(hv)_{i+\frac{1}{2},j}$, and add the results. With the forms given by (9.128) and (9.129), the vorticity terms will sum to

$$
\begin{aligned}
&-(hu)_{i,j+\frac{1}{2}}\left[\left(\frac{\zeta+f}{h}\right)(hv)\right]_{i,j+\frac{1}{2}} + (hv)_{i+\frac{1}{2},j}\left[\left(\frac{\zeta+f}{h}\right)(hu)\right]_{i+\frac{1}{2},j} \\
&= -(hu)_{i,j+\frac{1}{2}}\Big[\alpha_{i,j+\frac{1}{2};i+\frac{1}{2},j+1}(hv)_{i+\frac{1}{2},j+1} + \beta_{i,j+\frac{1}{2};i-\frac{1}{2},j+1}(hv)_{i-\frac{1}{2},j+1} \\
&\qquad + \gamma_{i,j+\frac{1}{2};i-\frac{1}{2},j}(hv)_{i-\frac{1}{2},j} + \delta_{i,j+\frac{1}{2};i+\frac{1}{2},j}(hv)_{i+\frac{1}{2},j}\Big] \\
&\quad + (hv)_{i+\frac{1}{2},j}\Big[\gamma_{i+\frac{1}{2},j;i+1,j+\frac{1}{2}}(hu)_{i+1,j+\frac{1}{2}} + \delta_{i+\frac{1}{2},j;i,j+\frac{1}{2}}(hu)_{i,j+\frac{1}{2}} \\
&\qquad \alpha_{i+\frac{1}{2},j;i,j-\frac{1}{2}}(hu)_{i,j-\frac{1}{2}} + \beta_{i+\frac{1}{2},j;i+1,j-\frac{1}{2}}(hu)_{i+1,j-\frac{1}{2}}\Big] \ .
\end{aligned}
\tag{9.130}
$$

Inspection of (9.130) makes it clear that cancellation will occur when we sum over the grid. This means that the vorticity terms will drop out of the finite-difference kinetic energy equation, just as they drop out of the continuous kinetic energy equation. This cancellation will occur regardless of the expressions that we choose for the mass fluxes, and regardless of the expressions that we choose for the α's, β's, γ's, and δ's. The cancellation arises purely from the forms of (9.128) and (9.129), and is analogous to the cancellation that makes (9.121) work, i.e.

$$
A\mathbf{V} \bullet (\mathbf{k} \times \mathbf{V}) = A(u\mathbf{i} + v\mathbf{j}) \bullet (-v\mathbf{i} + u\mathbf{j}) = A(-uv + uv) = 0 \ , \tag{9.131}
$$

regardless of the input quantities A and $\mathbf{V}$. This is yet another example of "mimetic

discretization."

The above discussion shows that the finite-difference momentum equations represented by (9.126) and (9.126) with the use of (9.128) and (9.129) will guarantee kinetic energy conservation under advection, regardless of the forms chosen for the mass fluxes and the interpolated potential vorticities α, β, γ, and δ. From this point, the methods used in the discussion of the one-dimensional purely divergent flow will carry through essentially without change to give us conservation of mass, potential energy, and total energy.

Arakawa and Lamb (1981) went much further, however, showing how the finite-difference momentum equations presented above (or, actually, slightly generalized versions of these equations) allow conservation of both potential vorticity and potential enstrophy. The details are rather complicated and will not be presented here.

9.7 The effects of time differencing on energy conservation

A family of finite-difference schemes for (9.13) can be written in the generic form

$$\frac{q_{i,j}^{n+1} - q_{i,j}^{n}}{\Delta t} = J_{i,j}(q^{*}, \psi), \tag{9.132}$$

where $J_{i,j}$ is a finite difference analog to the Jacobian at the point (i, j), and different choices of q^{*} give different time-differencing schemes. Examples are given in Table 9.1. Multiplying

Table 9.1: Examples of time differencing schemes obtained through various choices of q^{*}. The subscripts i and j have been omitted for simplicity.

Name of Scheme	Form of Scheme
Euler (forward)	$q^{*} = q^{n}$
Backward implicit	$q^{*} = q^{n+1}$
Trapezoidal implicit	$q^{*} = \frac{1}{2}(q^{n} + q^{n+1})$
Leapfrog (here the time interval is $\Delta t/2$)	$q^{*} = q^{n+\frac{1}{2}}$
Second-order Adams Bashforth	$q^{*} = \frac{3}{2}q^{n} - \frac{1}{2}q^{n-1}$

Table 9.1: Examples of time differencing schemes obtained through various choices of q^*. The subscripts i and j have been omitted for simplicity.

Name of Scheme	Form of Scheme
Heun	$q^* = q^n + \frac{\Delta t}{2} J(q^n, \psi)$
Lax-Wendroff *(here S is a smoothing operator)*	$q^* = Sq^n + \frac{\Delta t}{2} J(q^n, \psi)$
Matsuno	$q^* = q^n + \Delta t J(q^n, \psi)$

(9.132) by q^*, we get

$$q^*(q^{n+1} - q^n) = \Delta t q^* J(q^*, \psi) , \tag{9.133}$$

or, after some algebraic sleight-of-hand,

$$(q^{n+1})^2 - (q^n)^2 = 2\left(\frac{q^{n+1} + q^n}{2} - q^*\right)(q^{n+1} - q^n) + 2\Delta t q^* J(q^*, \psi) . \tag{9.134}$$

The left-hand side of (9.134) represents the change of q^2 in one time step. Consider the summation of q^2 over all grid points, divided by the number of grid points, and let this mean be denoted by an overbar. We find that

$$\overline{(q^{n+1})^2} - \overline{(q^n)^2} = 2\overline{\left(\frac{q^{n+1} + q^n}{2} - q^*\right)(q^{n+1} - q^n)} + 2\Delta t \overline{q^* J(q^*, \psi)} , \tag{9.135}$$

which shows that the change of the mean-square of q depends on two terms. The first term involves the choice of q^*. For $q^* = q^n$, the contribution of this term is positive, while for $q^* = q^{n+1}$, it is negative. If we use the trapezoidal scheme, which is an absolutely stable and neutral scheme (in the linear case with constant coefficients), there is no contribution from the first term. This means that the trapezoidal scheme is consistent with (allows) exact energy conservation. Of course, the form of the finite-difference Jacobian must also be consistent with energy conservation.

In most cases, time truncation errors which interfere with exact energy conservation do not cause serious problems, provided that the scheme is stable in the linear sense, e.g. as indicated by von Neuman's method.

9.8 Summary

We began this chapter by discussing two-dimensional advection. When the advecting current is variable, a new type of instability can occur, which is best called "aliasing instability." In practice, it is often called "non-linear instability." This type of instability occurs regardless of the time step, and cannot be detected by von Neuman's method. It can be detected by the energy method (see Chapter 2), and it can be controlled by enforcing conservation of appropriate quadratic variables, such as energy or enstrophy. It is particularly likely to cause trouble with the momentum equations, which describe how the wind is "advected by itself." Conservation of potential vorticity is an extremely important dynamical principle, as discussed in courses on atmospheric dynamics. Conservation of potential enstrophy is key to determining the distribution of kinetic energy with scale. Schemes which permit conservation of potential vorticity and potential enstrophy under advection therefore provide major benefits in the simulation of geophysical circulations.

Problems

1. A wagon wheel rotates at R revolutions per second. It is featureless except for a single dot painted near its outer edge. The wheel is filmed at r frames per second.

   a) What inequality must r satisfy to avoid aliasing?

   b) What rotation rate does a person watching the film see, for given values of r and R?

   c) Under what conditions does the wheel appear to turn "backwards?"

2. a) Starting from the continuous equation

$$\frac{\partial \xi}{\partial t} = J(\xi, \psi) , \tag{9.136}$$

   prove that kinetic energy is conserved for two-dimensional nondivergent flow. Assume periodic boundary conditions.

   b) Repeat for J_3. Use an exact time derivative.

3. Prove that J_2 gives exact vorticity conservation (ignoring time truncation error). Assume periodic boundary conditions.

4. Work out the *continuous* form of the Jacobian for the case of spherical coordinates (longitude λ and latitude φ).